JVC

Journal of Vibration and Control
000(00) 1–12

DOI: 10.1177/1077546309349848
jvc.sagepub.com
SAGE

Stability Analysis of a Nonlinear Jointed Beam under Distributed Follower Force

H. Ahmadian and H. Azizi

Abstract

This paper deals with the stability of a beam subjected to thrust. The thrust acts upon the structure as a follower non-conservative force, thus the structure can lose its stability by flutter or divergence depending on the system parameters. The model consists of two beams interconnected by a nonlinear joint. The joint is a combination of linear and nonlinear springs and a damper. Follower force is assumed to be linearly distributed along the length of beam, so the governing equation has variable coefficients, so that only an approximate solution is possible. We divided the beam into a number of segments so that force distributions could be approximated as constants and then we used the method of multiple scales to obtain the analytical solution of the system. The flutter and divergence and post-critical behavior are then obtained.

Keywords

Bifurcation analysis, divergence, flutter, method of multiple scales

Received XX 200X; accepted 19 August 2009

Introduction

Free-free beams have been intensively exploited to simulate the stability behavior of flexible missiles and/or space structures propelled by end rocket thrust. Beal's paper (Beal, 1965) deals with a uniform beam under constant and pulsating thrust including a simplified control system. Due to the non-conservative nature of the end thrust a consistent dynamic analysis is needed to predict correctly the stability behavior (Bolotin, 1963; Barsoum, 1973).

However, different critical behaviors arise if non-conservative loads (e.g. follower forces) are applied, such as those caused by the thrust of rocket and jet engines, dry friction in automotive disk and drum-brake systems. Under these circumstances the loss of stability may happen either by divergence or by flutter, depending on the mechanical properties of the structure. In addition, when conservative and non-conservative loads are applied simultaneously, the critical boundaries in the control parameters space show an interaction phenomenon (Langthjem and Sugiyama, 2000). Namely, the critical conservative load increases in the presence of non-conservative forces, while the critical non-conservative load decreases in the presence of conservative forces. Several reviews of problems involving non-conservative forces have been published (Herrmann, 1967; Sundararaian, 1975) as well as books on this subject, (Panovko and Gubanova, 1965; Ziegler, 1968; Leipholz, 1980; Bazant and Cedolin, 1991). However, the attention has been mainly focused on the linear stability analysis and very little over the post-critical behavior. Recently the authors devoted particular attention to the study of multiple dynamic bifurcation points for discrete systems (Luongo et al., 2002). Paolone et.al. (2006) analyzed the stability of a cantilever elastic beam under the action of a follower tangential force and a bending conservative couple at the free end. Nonlinear, partial integro-differential equations of motion are derived and expanded up to cubic terms in the transversal displacement and torsional angle of the beam. They also studied the linear stability of the trivial equilibrium, revealing the existence of buckling, flutter and double-zero critical points. Then the post-critical behavior of a cantilever beam under simultaneous action of conservative and non-conservative loads was analyzed. The bifurcation equations for simple buckling (divergence), simple flutter (Hopf) and double-zero (Takens–Bogdanova–Arnold) bifurcations are derived by means of the multiple time scales method. Finally, some numerical results are derived and the bifurcation scenario of the beam is discussed.

Mladenov and Sugiyama (1997) considered a free-free, flexible two-beam system, where the two beams are connected by two springs and two dampers, one of each (coupled in parallel) for the rotational motion, and one of

Department of Mechanical Engineering, Iran University of Science and Technology, Narmak, Tehran 16844, Iran (azizi@eied.com)

each for the parallel motion. Bending-flutter, post-flutter-divergence and folding instability may occur, depending on the system parameters.

The effect of axial compressive inertia forces due to large thrust/accelerations in a variable geometry, variable mass single stage rocket has been investigated by Joshi (1995). Starting from an elementary beam formulation for variable geometry rocket subjected to variable axial compressive inertia forces, solutions for the transverse vibration have been obtained by converting the variable coefficient governing equation into a set of constant coefficient equations by dividing the rocket structure into piecewise constant property segments. The exact solution for vibration was obtained within these segments by using beam functions. The results obtained for a typical single stage rocket bring out the fact that the axial compressive forces arising, due to thrust, significantly lower the transverse vibration frequencies of practical variable mass rockets.

Ahmadian and Jalali (2007) have presented a nonlinear model for bolted lap joints and interfaces that is capable of representing the dominant physics involved in the joint such as micro/macro-slip. The joint interface was modeled using a combination of linear and nonlinear springs and a damper to simulate the damping effects of the joint. An estimate of the response of the structure with a nonlinear model for the bolted joint is obtained using the method of multiple scales. The parameters of the model, i.e. the spring constants and the damper coefficient, are functions of normal and tangential stresses at the joint interface and are identified by minimizing the difference between the model predictions and the experimentally-measured data. The model that is utilized in this paper is exactly the same as Ahmadian and Jalali's nonlinear model for lap joints.

Model

The bolted structure considered in this work is shown in Figure 1. It includes two identical linear Euler-Bernoulli free-free beams connected at one of their free ends by a bolted joint. The bolted joint interface is modeled with a nonlinear spring which resembles the softening effect of the joint interface at certain level of stresses in the interface by using the results of Ahmadian and Jalali (2007). The Euler–Bernoulli beam assembly considered here has a nonlinear flexibility at x = L/2 (see Figure 1). The equations of motion for each part of the beam are:

$$EI\,\frac{\partial^4 W_1(x,t)}{\partial x^4}+m\frac{\partial^2 W_1(x,t)}{\partial t^2}+P(x)\frac{\partial^2 W_1(x,t)}{\partial x^2} = F(t)\,\delta(x)\;;\quad 0<x<S\quad EI\frac{\partial^4 W_2(x,t)}{\partial x^4} + m\frac{\partial^2 W_2(x,t)}{\partial t^2}+P(x)\frac{\partial^2 W_2(x,t)}{\partial x^2}=0\;;\quad S<x<L \tag{1}$$

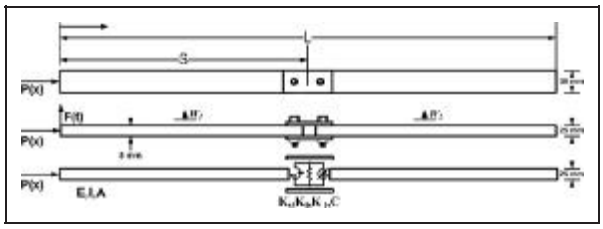

Figure 1. The free-free beam/model with a lap joint.

where *EI, m*, $W_1(x,t)$, $W_2(x,t)$, *F(t)* and *P(x)* are flexural rigidity, linear mass density, lateral displacement at each of the two parts of the beam, and the point excitation on the beam at $x = 0$ and the follower force, respectively. The boundary conditions of the problem are defined as

$$\frac{\partial^2 W_1(0,t)}{\partial x^2}=\frac{\partial^3 W_1(0,t)}{\partial x^3}=0,\quad \frac{\partial^3 W_2(L,t)}{\partial x^3}=\frac{\partial^2 W_2(L,t)}{\partial x^2}=0, \tag{2}$$

Next we turn our attention to the equilibrium requirements at the joint interface. To simplify the problem, one may neglect the mass effects of the joint interface and equate the bending moments and the shear forces of the two beam parts at the interface as

$$\frac{\partial^2 W_1(S,t)}{\partial x^2}=\frac{\partial^2 W_2(S,t)}{\partial x^2},\quad \frac{\partial^3 W_1(S,t)}{\partial x^3}=\frac{\partial^3 W_2(S,t)}{\partial x^3},$$
$$-EI\frac{\partial^3 W_1(S,t)}{\partial x^3}=K_1(W_2(S,t)-W_1(S,t)),$$
$$EI\frac{\partial^2 W_1(S,t)}{\partial x^2}=C\left(\frac{\partial^2 W_2(S,t)-\partial^2 W_1(S,t)}{\partial x\partial t}\right)+K_\theta\left(\frac{\partial W_2(S,t)-\partial W_1(S,t)}{\partial x}\right)-K_3\left(\frac{\partial W_2(S,t)-\partial W_1(S,t)}{\partial x}\right)^3. \tag{3}$$

where K_1, K_θ, K_3 and *C* are linear translational spring, linear torsional spring, cubic torsional spring and torsional viscous damper of joint, respectively. The values of these parameters are tabulated in Table 1. The cubic stiffness and viscous damping terms represent the saturation phenomenon and energy loss at the joint interface in the presence of high-level vibrations. In the following, a solution to the above problem using the method of multiple scales is presented.

The Analytical Solution

In this section, a solution of the governing equations stated in equation (1), satisfying the equilibrium requirements at the joint (equation (3)), along with the associated boundary conditions is sought (equation (2)). The method of multiple

Table 1. The joint and beam parameters.

m (Kg/m)	C (N.s/m)	$K3$ (N/m3)	K_l (N /m)	K_θ (N /rad)
2.145	0.281	3.72e8	8.09e8(1+0.05i)	3264(1+0.05i)

scales is applied directly to these equations. Solutions for each part of the beam are assumed of the forms:

$$\begin{aligned} W_1(x,t;\varepsilon) &= W_{10}(x,T_0,T_1) + \varepsilon W_{11}(x,T_0,T_1), \\ W_2(x,t;\varepsilon) &= W_{20}(x,T_0,T_1) + \varepsilon W_{21}(x,T_0,T_1), \end{aligned} \tag{4}$$

where $T_0 = t$ is the fast time scale, and $T_1 = \varepsilon t$ is the slow time scale. Behavior of the system is investigated near the resonance frequency. The linear undamped theory will predict unbounded oscillations at the resonance point no matter how small the excitation force is. In the considered system these large oscillations are limited by the damping and nonlinearity. Thus to obtain a uniformly valid approximate solution of this problem, one needs to order the excitation so that it will appear when the damping and the nonlinearity appear (Ahmadian and Jalali, 2007). Therefore the forcing function, the nonlinear stiffness and the damping due to micro-slips are ordered as

$$\frac{F}{m} = \varepsilon f, \frac{C}{m} = \varepsilon \mu, \frac{K_3}{m} = \varepsilon K_N. \tag{5}$$

The derivatives with respect to the new time scales are defined as

$$\frac{d}{dt} = D_0 + \varepsilon D_1, \quad \frac{d^2}{dt^2} = D_0^2 + 2D_0D_1, \quad D_n = \frac{\partial}{\partial T^n}. \tag{6}$$

Inserting the new variables into the system equations and sorting the obtained equations based on the orders of ε one obtains:

Order ε^0

The governing equations:

$$\begin{aligned} D_0^2 W_{10} + \frac{P(x)}{m} W_{10}^{II} + \frac{EI}{m} W_{10}^{iv} = 0, \\ D_0^2 W_{20} + \frac{P(x)}{m} W_{20}^{II} + \frac{EI}{m} W_{20}^{iv} = 0. \end{aligned} \tag{7}$$

With boundary conditions:

$$\begin{aligned} W_{10}^{'''}(0,T_0,T_1) = W_{10}^{'}(0,T_0,T_1) = 0, \\ W_{20}^{'''}(L,T_0,T_1) = W_{20}^{''}(L,T_0,T_1) = 0, \end{aligned} \tag{8}$$

And equilibrium conditions:

$$\begin{aligned} &W_{10}^{'''}(S,T_0,T_1) = W_{20}^{'''}(S,T_0,T_1), W_{10}^{''}(S,T_0,T_1) = W_{20}^{''}(S,T_0,T_1), \\ &EI\, W_{10}^{''}(S,T_0,T_1) = K_\theta(W_{20}^{'}(S,T_0,T_1) - W_{10}^{'}(S,T_0,T_1)), \\ &EI\, W_{10}^{'''}(S,T_0,T_1) = K_1(W_{10}(S,T_0,T_1) - W_{20}(S,T_0,T_1)), \end{aligned} \tag{9}$$

Order ε^1.

The governing equations:

$$\begin{aligned} &D_0^2 W_{11} + \frac{P(x)}{m} W_{11}^{II} + \frac{EI}{m} W_{11}^{iv} \\ &\quad = -2D_0D_1W_{10} + f\cos(\Omega t)\delta(0), \\ &D_0^2 W_{21} + \frac{P(x)}{m} W_{21}^{II} + \frac{EI}{m} W_{21}^{iv} = -2D_0D_1W_{20}. \end{aligned} \tag{10}$$

The boundary conditions:

$$\begin{aligned} W_{11}^{'''}(0,T_0,T_1) = W_{11}^{''}(0,T_0,T_1) = 0, \\ EI\, W_{21}^{'''}(L,T_0,T_1) = W_{21}^{''}(L,T_0,T_1) = 0, \end{aligned} \tag{11}$$

And equilibrium conditions:

$$\begin{aligned} W_{11}^{'''}(S,T_0,T_1) = W_{21}^{'''}(S,T_0,T_1), \\ W_{11}^{''}(S,T_0,T_1) = W_{21}^{''}(S,T_0,T_1). \end{aligned} \tag{12}$$

$$\begin{aligned} \frac{EI}{m} W_{11}^{''}(S,T_0,T_1) &= \mu D_0(W_{20}^{''}(S,T_0,T_1) - W_{10}^{''}(S,T_0,T_1)) \\ &+ \frac{K_\theta}{m}(W_{21}^{'}(S,T_0,T_1) - W_{11}^{'}(S,T_0,T_1)) \\ &- K_N(W_{20}^{'}(S,T_0,T_1) - W_{10}^{'}(S,T_0,T_1))^3, \\ EI\, W_{11}^{'''}(S,T_0,T_1) &= K_1(W_{11}(S,T_0,T_1) - W_{21}(S,T_0,T_1)). \end{aligned}$$

Where $()' = \partial/\partial x$.

Linear Solution

Assuming the response of the structure is dominated by a single mode, $Y_i(x)$, one may write the solution to the set of equations of order ε^0as

$$\begin{aligned} W_{10}(S,T_0,T_1) &= (A(T_1)e^{i\omega T_0} + cc)\, Y_1(x), \\ W_{20}(S,T_0,T_1) &= (A(T_1)e^{i\omega T_0} + cc)\, Y_2(x), \end{aligned} \tag{13}$$

where ω is the natural frequency of the structure and cc is the complex conjugate term for each part of the solution. The assumed solution transforms zero order equations to the following form:

$$Y_i^{iv} + \frac{P(x)}{EI} Y_i^{II} - \lambda^4 Y_i = 0, \quad i = 1, 2, \quad \lambda^4 = \frac{m\omega^2}{EI}. \tag{14}$$

It can be seen that the governing equation in this case has variable coefficients, namely the axial follower force $P(x)$. It is clear, therefore, that only an approximate solution is possible. An iterative scheme for solving equations with variable coefficients, based on Galerkin's formulation, has been described in many papers (Beal, 1965; Wu, 1975). However, in the present case it is more convenient to use beam functions along with finite segments in view of the fact that admissible functions satisfying the boundary conditions (Joshi, 1995). Therefore, in the present study the structure is divided into a number of segments, within which the follower force can be approximated as constants. Such an approach has the advantage that it is capable of taking into account fairly complex beam configurations just by increasing the number of segments. Furthermore, these simplifications lead to governing equations with constant coefficients which can be solved exactly in terms of beam functions. The non-dimensional equation of motion for the i th constant beam segment can then be written as:

$$(\partial^4 Y_i/\partial \bar{x}_i^4) + a_i(\partial^2 Y_i/\partial \bar{x}_i^2) - \lambda^4 Y_i = 0 \qquad i = 1 : N. \tag{15}$$

Here $a_i \{= P(x_i)L^2/(EI)\}$ is the dimensionless follower force and $\lambda^4 \{= m\omega^2 L^4/(EI)\}$ is the dimensionless frequency parameter for the i th segment. The variable $\bar{x}_i$ is the dimensionless length coordinate such that it takes values from 0 to $l\,(= L/N)$ for all segments, where $l$is the length of each segment. The follower force $P(x_i)$ is defined as the inertia compressive force acting on the i th beam segment and is calculated at the centre of gravity of the segment by summing up the inertias of all the segments preceding the current one and taking the average inertia force for the current segment. The expressions for $P(x_i)$for the constant acceleration trajectory can be written as

$$\begin{aligned} P(x_i) &= a\rho A\,(0.5l + \sum_{1}^{i-1} l) \\ a &= P/(mL) \end{aligned} \tag{16}$$

where a is the constant acceleration. The general solution of equation (15) can be written in terms of beam functions as

$$\begin{aligned} Y_i = A_i \cosh \lambda_{1i}\bar{x}_i + B_i \sinh \lambda_{1i}\bar{x}_i + C_i \cos \lambda_{2i}\bar{x}_i \\ + D_i \sin \lambda_{2i}\bar{x}_i, \end{aligned} \tag{17}$$

where A_i, B_i, C_i and D_i are arbitrary constants and λ_{1i} and λ_{2i} are roots of the characteristic equation for each segment, obtained as

$$\lambda_{1i}^2 = \left\{(a_i^2 + 4\lambda^4)^{1/2} - a_i\right\}/2, \qquad \lambda_{2i}^2 = \left\{(a_i^2 + 4\lambda^4)^{1/2} + a_i\right\}/2. \tag{18}$$

It is to be noted here that there will be a total of 4N unknown coefficients for N segments. The characteristic equation for the natural frequencies is obtained by applying the boundary conditions at the two ends of the beam and continuity conditions between the segments of the beam. The boundary conditions are

$$Y_1''(0) = Y_1'''(0) = 0, \qquad Y_N''(l) = Y_N'''(l) = 0; \tag{19}$$

The continuity conditions are

$$\begin{aligned} &Y_i(l) = Y_{i+1}(0), \quad Y_i'(l) = Y_{i+1}'(0), \quad i = 1 : N-1, \quad i \neq N/2 \\ &Y_i''(l) = Y_{i+1}''(0), \quad Y_i'''(l) = Y_{i+1}'''(0), \end{aligned} \tag{20}$$

And continuity conditions in joint are

$$\begin{aligned} &Y_i''(l) = Y_{i+1}''(0), \qquad Y_i'''(l) = Y_{i+1}'''(0), \qquad i = N/2 \\ &Y_i''(l) = \frac{K_\theta}{EI}(Y_{i+1}'(0) - Y_i'(l)), \qquad Y_i'''(l) = \frac{K_1}{EI}(Y_i(l) - Y_{i+1}(0)), \end{aligned} \tag{21}$$

It can be seen that there are four boundary conditions and 4(N–1) continuity conditions. The transcendental characteristic equation is represented by a 4N × 4N determinant the zeros of which give various values of the frequency parameter λ. These values of λ are obtained by the Regula-Falsi method of locating zeroes of a function. This involves identifying the sign change of the function for two trial values of λ at which point the gap is closed successively until convergence is reached. In the present case, convergence is assumed to be reached if the difference between the two values of λ is found to be less than 0.001. The converged value of the frequency parameter λ is then used for generating the free vibration mode shape. It is to be mentioned here that, as the governing equations have variable coefficients, the accuracy of the converged eigenvalues also depends on the number of segments included in the solution.

The numerical exercise in the present study has been carried out with the help of a total of sixteen segments of constant force as an acceptable approximation of the complex full scale beam.

Convergence results in Table 2 show the accuracy of modeling the linearly varying inertia force approximately as stepwise constant. It is seen that with only twelve segments, the analysis shows convergence for frequency.

Mode shapes of system shown in Figure 2 for three variables of force. It is seen that by increasing value of force, lateral displacement of beam decreases.

For checking the validity of the numerical results in this procedure, we compare the flutter with the results of the

Table 2. Convergence of solution for variable follower force versus number of segments.

	P = 0			P = 5000			P = 10000		
N	ω1	ω2	ω3	ω1	ω2	ω3	ω1	ω2	ω3
2	104.96	323.38	603.88	89.12	313.07	589.63	73.07	295.87	570.45
4	104.96	323.38	603.88	89.92	312.24	591.41	73.45	295.32	573.22
8	104.96	323.38	603.88	90.02	309.52	587.32	74.48	290.14	569.45
12	104.96	323.38	603.88	91.51	306.03	585.91	75.61	287.39	567.31
16	104.96	323.38	603.88	91.51	306.03	585.91	75.61	287.39	567.31

Beal (1965). By taking very large values for the joint's springs and very small value for damper of the joint, we force the free-free beam's boundary conditions. The branches of first and second non-dimensional natural frequencies are plotted in Figure 3. As shown in Figure 3, the results are shown have good coincidence with result of Beal (1965).

Buckling. As well known, for the evaluation of the critical buckling boundaries, it is sufficient to consider only the linear static parts of equation (15) or let $\lambda = 0$. The following ordinary differential equation is obtained:

$$(\partial^4 Y_i/\partial \bar{x}_i^4) + a_i(\partial^2 Y_i/\partial \bar{x}_i^2) = 0 \qquad i = 1:N. \tag{22}$$

Solution of equation (22) returns

$$Y_i = A_i + B_i x + C_i \cos \lambda_i \bar{x}_i + D_i \sin \lambda_i \bar{x}_i, \qquad \lambda_i = \sqrt{a_i}. \tag{23}$$

Inserting equation (22) into the boundary and continuity conditions, a homogeneous linear system is obtained, by expanding the determinant and setting it equal to zero, the critical buckling force is obtained that is equal to 102475 N.

Flutter. Flutter occurs when the linear motion is harmonic, i.e. the eigenvalue is purely imaginary $\lambda = i\omega$ where ω is the non-dimensional linearized small oscillation frequency; or two natural frequencies are equal. By setting $\lambda = i\omega$ in equation (15) and similar to the buckling in 3.2.1 expanding the determinant and setting it equal to zero, the critical flutter force is obtained. For the second approach, we plot the natural frequencies versus value of force, so the flutter occurs as a result of the coalescence of the characteristic frequencies. Where one branch reaches the horizontal axis, divergence instability occurs. The results are shown in Figure 4. In Figure 4(a), the absolute of natural frequencies are plotted versus follower force and the real parts of them are plotted in Figure 4(b). It is shown that the first flutter force is 22587.5 N and the second flutter force is 42965 N. They are obtained respectively by the first and second approaches explained above. Divergence mode shape is plotted in Figure 5. Figure 6 shows the real and imaginary mode shape of first flutter instability.

Adjoint Problem

It is necessary to solve the adjoint problem of the linearized equation (7), useful to enforce solvability conditions. For the purpose of computing this adjoint, we will define the following inner product:

$$\langle f, g \rangle = \int_0^L f^* g(s) ds. \tag{24}$$

The adjoint of our linear operator L^*satisfies the following inner product:

$$\langle \psi, L(\phi) \rangle = \langle L^*(\psi), \phi \rangle \quad \textit{where} \quad L(\phi) = \phi^{IV} + P(x)\phi^{II}, \tag{25}$$

Taking the inner product of an arbitrary function of adjoint ψ with the linear operator L, we obtain

$$\langle \psi, L(\phi) \rangle = \int_0^L \psi(\phi'''' + (P)\phi'') ds. \tag{26}$$

We can obtain the adjoint linear operator by repeatedly integrating this equation; see that the linear operator of adjoint system L^* is same as the L. The detail of integration, boundary and equilibrium conditions for adjoint system are obtained (see Appendix A). The free mode shapes of adjoint system are shown in Figure 7. Because of new boundary conditions and equilibrium condition the joint doesn't affect to free mode shapes, but by increasing the follower force, mode shapes have been affected by joint.

Nonlinear Solution

The homogeneous equation (7) has a non-trivial solution; therefore the non-homogeneous problem equations (10) to (12) will have a solution only if the solvability condition is satisfied. To determine this condition, the secular terms ϕ_i and non-secular terms V_i are separated by assuming a solution of the form:

$$\begin{aligned} W_{11} &= \varphi_1(x, T_1)e^{i\omega T_0} + V_1(x, T_0, T_1) + cc, \\ W_{21} &= \varphi_2(x, T_1)e^{i\omega T_0} + V_2(x, T_0, T_1) + cc, \end{aligned} \tag{27}$$

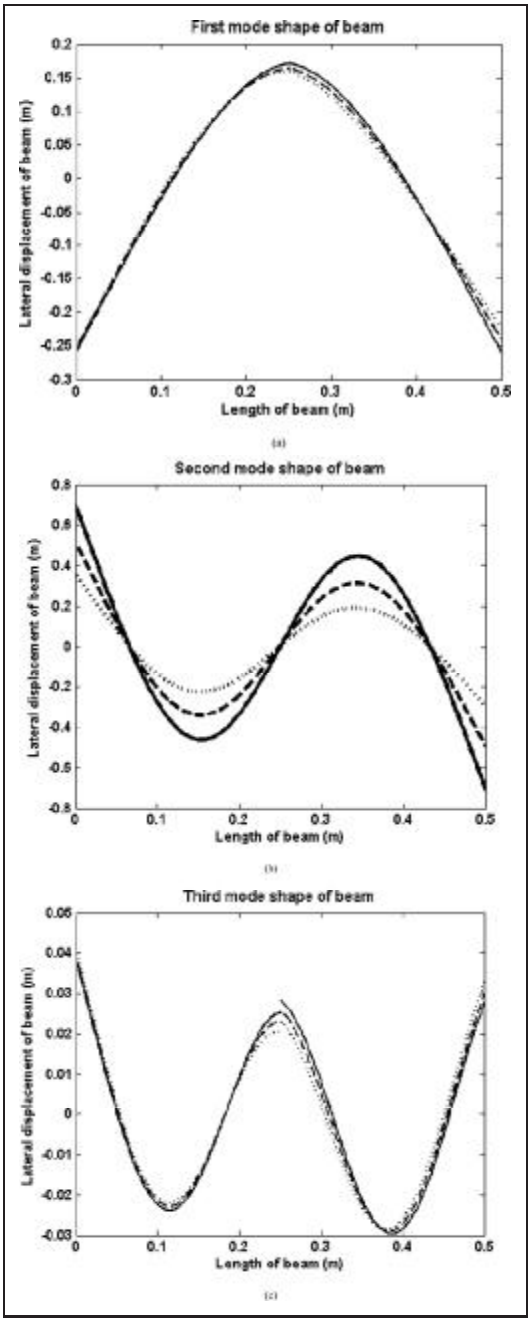

Figure 2. Mode shapes of beam versus 3 values for follower force. The full, dashed and dotted represent 0, 10000 and 20000 (N) respectively.

The excitation frequency Ω is assumed to be close to the natural frequency of the dominant mode which governs the system response, i.e.:

$$\Omega = \omega + \varepsilon\sigma; \tag{28}$$

Substituting equation (27) into the first-order equation (10), secular terms are obtained as

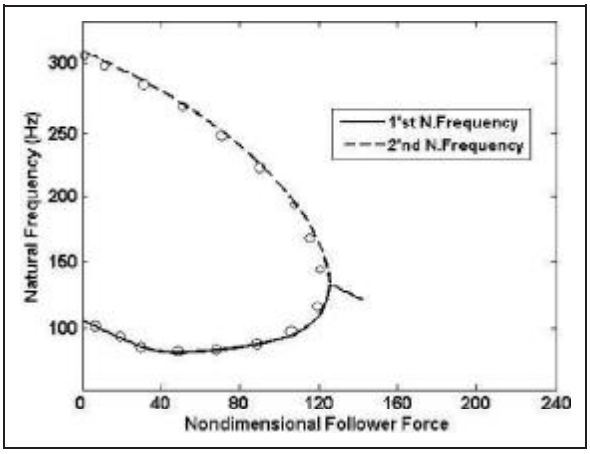

Figure 3. First and second branches of non-dimensional natural frequencies of free-free beam. The circle point denoted the result of Beal (1965).

$$\phi_1^{iv} + \frac{P(x)}{EI}\phi_1^{ii} - \lambda^4\phi_1 = \frac{f}{2}\delta(x)e^{i\sigma t} - 2\frac{i\omega}{EI}Y_1 D_1 A\ ;$$
$$\phi_2^{iv} + \frac{P(x)}{EI}\phi_2^{ii} - \lambda^4\phi_2 = -2\frac{i\omega}{EI}Y_2 D_1 A\ ; \tag{29}$$

By enforcing the solvability condition to equation (29), this equation obtained as

$$2i\omega_0\, m D_1 A = \mu i\omega_0(\varphi'_{AN/2+1} - \varphi'_{AN/2})(\varphi'_{1N/2+1} - \varphi'_{1N/2})$$
$$A - -\frac{3}{2}A^2\bar{A}K_N(\varphi'_{AN/2+1} - \varphi'_{AN/2})(\varphi'_{1N/2+1} - \varphi'_{1N/2})^2$$
$$(\bar{\varphi}'_{1N/2+1} - \bar{\varphi}'_{1N/2}) - \frac{f}{2}\varphi_{A1}(0)e^{i\sigma T_1}; \tag{30}$$

In extracting the solvability condition, one considers only the secular terms, i.e. the coefficient of $e^{i\omega T_0}$and its conjugate, and neglects the coefficient of the other harmonies such as the third-order super-harmony $e^{3i\omega T_0}$and its conjugate$e^{-3i\omega T_0}$. assuming for the complex amplitude *A(T1, . . .)* the polar form

$$A = \frac{1}{2}a(T_1)e^{i\beta(T_1)} \quad \gamma = \sigma T_1 - \beta. \tag{31}$$

By substituting equation (31) and separating real and imaginary part, in steady-state ($\dot{a} = \dot{\gamma} = 0$) equation (30) is simplified to the following response and frequency equation:

$$\frac{1}{2}\omega_0 Z(a' + i\beta')e^{i\beta} = \frac{1}{2}ia\mu\omega_0\, Qe^{i\beta} - \frac{1}{8}a^3 K_N S e^{i\beta}$$
$$-\frac{f}{2}\varphi_{A1}(0)e^{i\sigma T_1}a^2[(\frac{\mu Q}{Z})^2 + (\sigma + \frac{1}{4}\frac{K_N S\, a^2}{\omega_0 Z})^2] = \left(\frac{f\varphi_{1A}(0)}{\omega_0 Z}\right)^2 \tag{32}$$

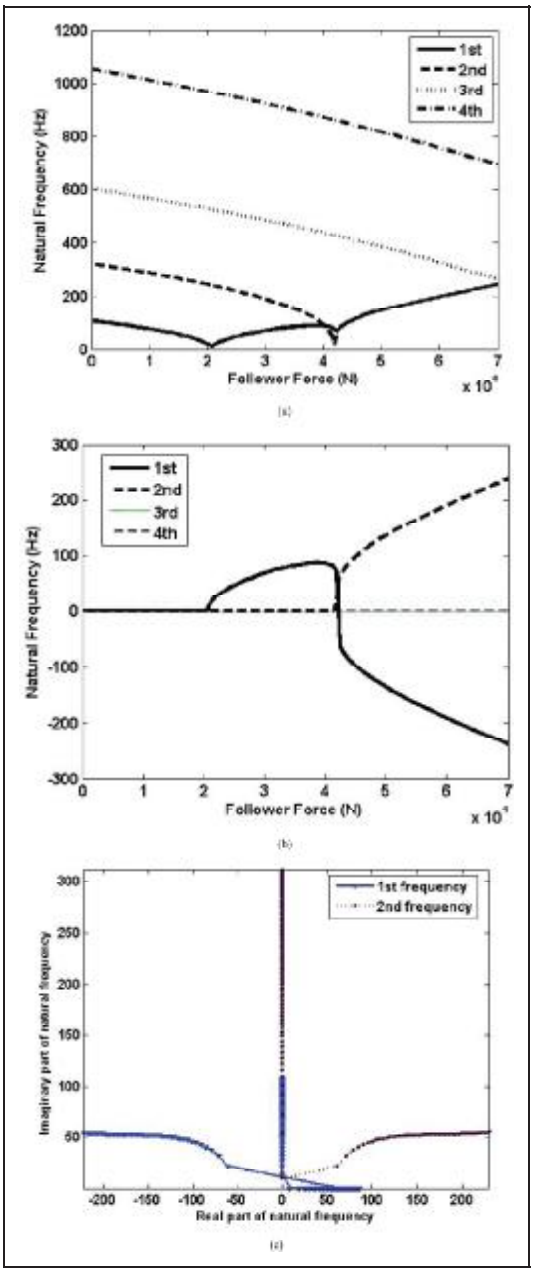

Figure 4. The branches of natural frequencies versus follower force. a) Absolute of frequencies. b) Real part of natural frequencies. c) Nyquist plot of first and second natural frequency.

where

$$Z = 2m; Q = (\varphi'_{AN/2+1} - \varphi'_{AN/2})(\varphi'_{1N/2+1} - \varphi'_{1N/2})\big|_{x=L/2};$$
$$S = \frac{3}{2}(\varphi'_{AN/2+1} - \varphi'_{AN/2})(\varphi'_{1N/2+1} - \varphi'_{1N/2})^2 (\bar{\varphi}'_{1N/2+1} - \bar{\varphi}'_{1N/2})\big|_{x=L/2}; \quad (33)$$

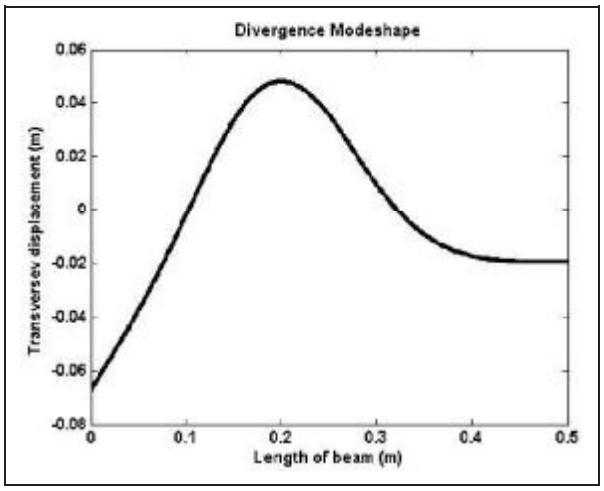

Figure 5. The divergence mode shape.

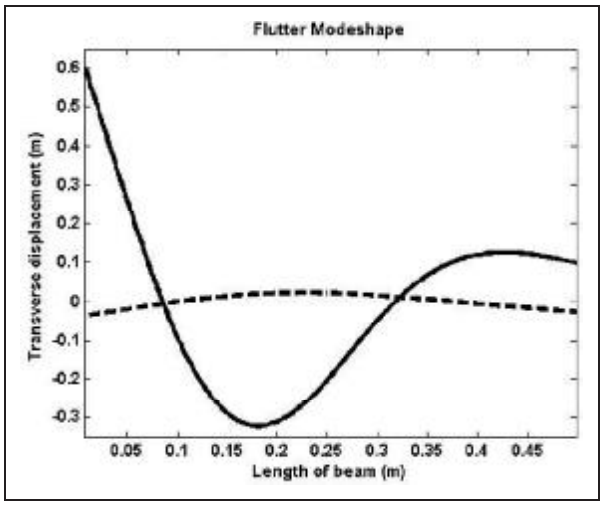

Figure 6. The flutter mode shape.solid line is real part and dashed line is imaginary part.

Equation (32) shows the dependency of amplitude and frequency in this case. a and β versus T_1 measured near first natural frequency of beam; with three value of force (0-4000–8000 N); are shown in Figures 8 and 9 respectively. It is seen that the joint has softening effect, because sign of β is minus. Too, by increasing the follower force, variation of amplitude α and phase β decrease.

The steady state amplitude (a) versus detuning parameter (σ) is shown in Figure 10. The curve clearly shows softening effect due to the joint properties. By increasing the follower force the softening effect of the joint vanishes.

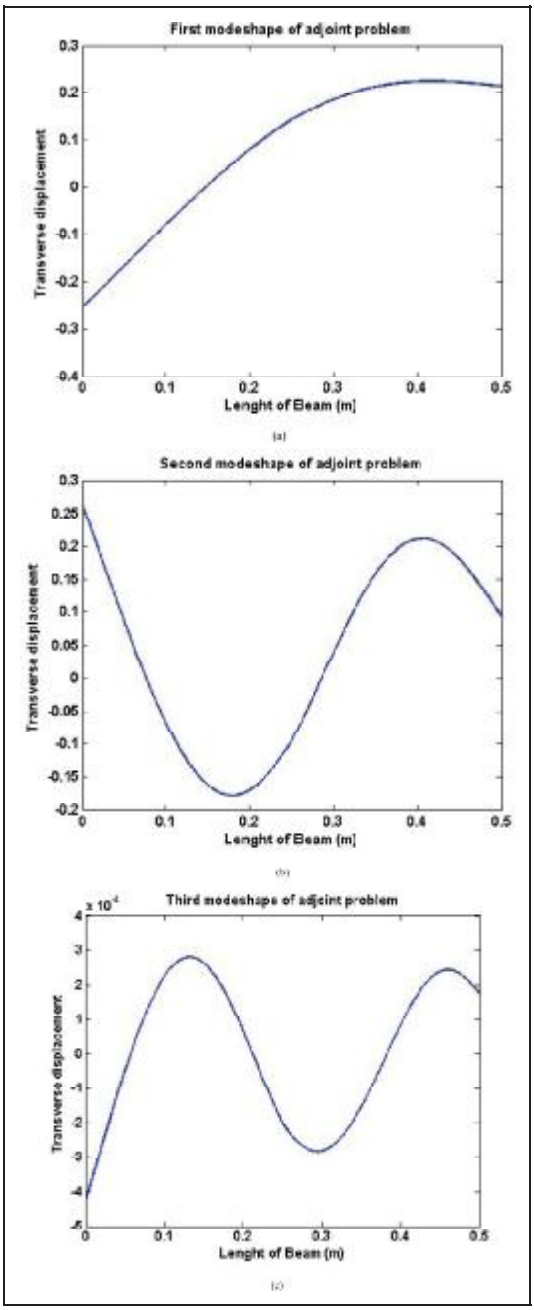

Figure 7. Free mode shapes of adjoint problem.

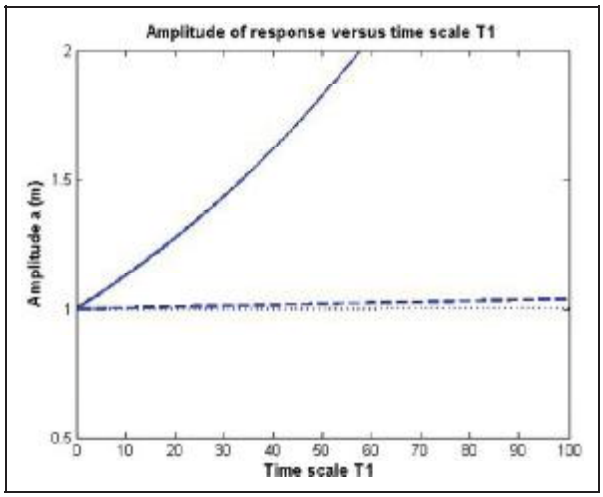

Figure 8. Amplitude of response versus time scale T_1. The full, dashed and dotted represent 0, 4000 and 8000 (N) respectively.

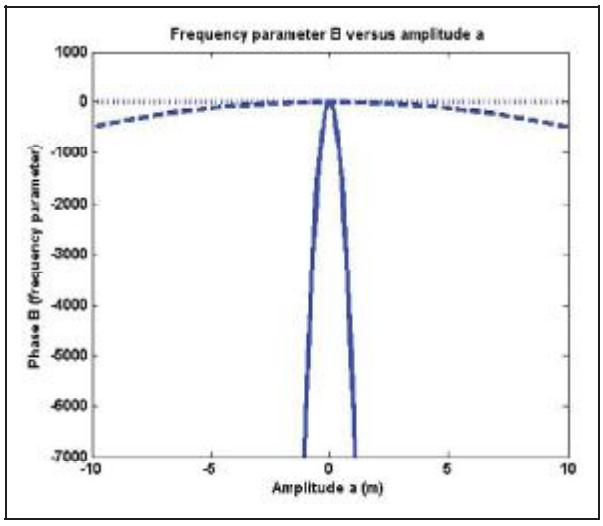

Figure 9. Frequency parameter β versus amplitude a. The full, dashed and dotted represent 0, 4000 and 8000 (N) respectively.

Stability Analysis

In this section, the post-critical analysis is performed for the two forms of instability, namely, around simple buckling (divergence) and simple flutter (Hopf).

Bifurcation Analysis

The multiple scale method is applied to analyze the system's behavior around a divergence point and Hopf point. Perturbation parameter ε, is introduced as a measure of the distance of a given point from the bifurcation point in the parameter follower force P.

Different ε-dependent time-scales $T_k = \varepsilon^k t$ are defined and the state variable Y(x) are expanded in Taylor series of ε. By equating terms of the same power of ε, linear perturbation equations having the same operator are obtained, and then solved in sequence for the series coefficients. Except for the lower-order eigenvalue problem, higher-order equations are nonhomogeneous; they admit a solution if and only if the known term belongs to the range of the singular operator, i.e. if it is orthogonal to the solutions of the adjoint homogeneous problem (26).

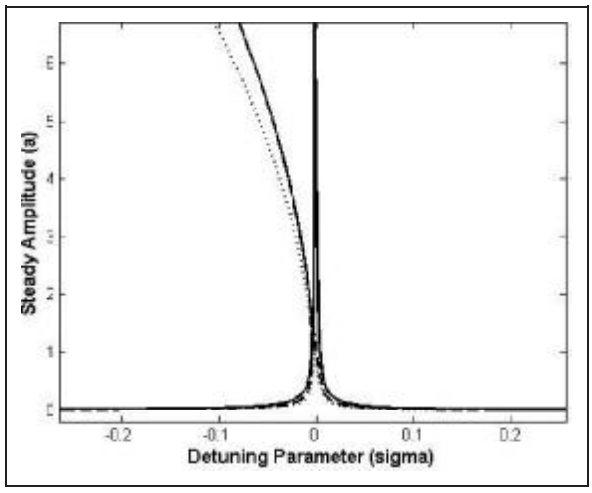

Figure 10. Steady state amplitude a versus detuning parameter σ. The full, dashed and dotted represent 0, 4000 and 8000 (N) respectively.

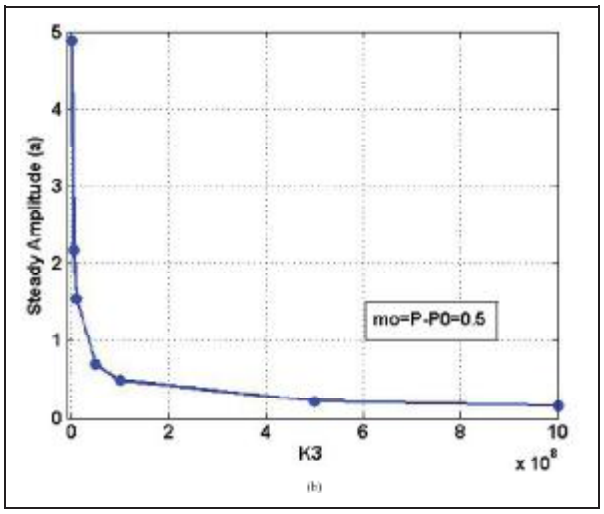

Figure 11. (a) Post-critical buckling steady amplitude behavior versus μ. (b) Amplitude α versus nonlinear stiffness K3.

The load P is taken as bifurcation parameter, and its deviation from the bifurcation value P_0 denoted by

$$\mu = P - P_0 = O(\varepsilon).$$

The equations of motion are rewritten as

$$\begin{aligned}
&\varepsilon^0 \ : \ (d^4 Y_{1i}/d\bar{x}_i^4) + a_i(d^2 Y_{1i}/d\bar{x}_i^2) + (\rho A/EI)D_0^2 Y_{1i} = 0 \\
&i = 1 : N \\
&\varepsilon^1 \ : \ (d^4 Y_{2i}/d\bar{x}_i^4) + a_i(d^2 Y_{2i}/d\bar{x}_i^2) + (\rho A/EI)D_0^2 Y_{2i} = \\
&-2(\rho A/EI)D_0 D_1 Y_{1i} \\
&-\mu(\partial a_i/\partial P)_{P_0}(d^2 Y_{1i}/d\bar{x}_i^2).
\end{aligned} \tag{34}$$

With the boundary and continuity conditions that are shown in Appendix B.

(a) Post buckling. When $\lambda = 0$, equation (34–1) furnishes $Y_{1i} = \alpha(T_1, \ldots)\varphi_i(x)$.Substituting this equation in equation (34–2) and boundary condition returns

$$\begin{aligned}
&(d^4 Y_{2i}/d\bar{x}_i^4) + a_i(d^2 Y_{2i}/d\bar{x}_i^2) + (\rho A/EI)D_0^2 Y_{2i} = \\
&\quad -2(\rho A/EI)\varphi_i D_1 \alpha - \mu(\partial a_i/\partial P)_{P_0}(d^2\varphi_i/d\bar{x}_i^2)\alpha.
\end{aligned} \tag{35}$$

By enforcing solvability condition, the following bifurcation equation for buckling is obtained

$$\dot{\alpha} = \mu R_1 \alpha + R_2 \alpha^3, \tag{36}$$

Where R_1 and R_2 are real parameters defined as follows:

$$\begin{aligned}
R_1 = &\frac{-EI}{2\rho A}\{\sum_{i=1}^{N}(\int_{l_{i-1}}^{l_i}\varphi_{Ai}(\frac{\partial a_i}{\partial P})_{P_0}\varphi_{1i}^2) - \sum_{i=1\neq N/2}^{N-1} \\
&[(\frac{\partial a_i}{\partial P})_{P_0}(\varphi_{Ai}\varphi_{1i} + \varphi'_{Ai}\varphi'_{1i}(l)) - (\frac{\partial a_{i+1}}{\partial P})_{P_0} \\
&(\varphi_{Ai+1}\varphi_{1i+1} + \varphi'_{Ai+1}\varphi'_{1i+1}(0))]\} \\
&+\frac{EI}{2\rho A}\{(\frac{\partial a_i}{\partial P})_{P_0}[\varphi_{Ai}\varphi_{1i}(0) + \varphi'_{Ai}\varphi'_{1i}(0)]\}_{i=1,N/2,N}; \\
R_2 = &\frac{-K_3}{2\rho A}(\varphi'_{AN/2+1} - \varphi'_{AN/2})(\varphi'_{1N/2+1} - \varphi'_{1N/2})^3;
\end{aligned} \tag{37}$$

In Figure 11(a), it is shown the bifurcation diagram obtained from the amplitude modulation equation, equation (36), in buckling points. From this Figure it clearly appears that the divergence bifurcations are of overcritical (stable) type, with the steady amplitude α decreasing with K_3. Hence, the variation of follower force has a stabilizing effect on the post-critical behavior as well as on the buckling linear boundary; and also, the curvature of the bifurcated paths changes monotonically with the bifurcation point. The nonlinearities are stronger for low values of K_3 and by increasing of K_3 nonlinearities will become weaker. This behavior is also appreciated in Figure 11(b), where the amplitude α is plotted versus the stiffness K_3 for a fixed value of the parameter μ.

(b) Post flutter. When $\lambda = i\omega_0$, equation (34–1) furnishes $Y_{1i} = A(T_1, \ldots)\varphi_i(x)e^{i\omega_0 T_0} + cc.$ where A($T1, \ldots$) is a complex amplitude and c.c. denotes complex conjugate. Substituting this equation in equation (34–2) and boundary condition returns

$$(d^4Y_{2i}/d\bar{x}_i^4) + a_i(d^2Y_{2i}/d\bar{x}_i^2) + (\rho A/EI)D_0^2Y_{2i} = -2i\omega_0(\rho A/EI)\varphi_i D_1 A - \mu(\partial a_i/\partial P)_{P_0}(d^2\varphi_i/d\bar{x}_i^2)A \quad (38)$$

By enforcing solvability condition and assuming for the complex amplitude *A(T1, ...)* the polar form

$$A = \frac{1}{2}a(T_1)e^{i\beta(T_1)} \quad (39)$$

the following bifurcation equation for the flutter is obtained

$$\dot{\alpha} = \mu C_1\alpha + C_2\alpha^3, \quad (40)$$

where $C1$and $C2$ are the real parts of the following complex coefficients, respectively:

$$\begin{aligned} C_1 &= D[\sum_{i=1}^{N}(\int_{l_i}^{l_i} \varphi_{Ai}(\frac{\partial a_i}{\partial P})_{P_0}\varphi_{1i}^2) - \sum_{i=1\neq N/2}^{N-1}[(\frac{\partial a_i}{\partial P})_{P_0}(\varphi_{Ai}\varphi_{1i} \\ &+ \varphi'_{Ai}\varphi'_{1i}(l)) - (\frac{\partial a_{i+1}}{\partial P})_{P_0}(\varphi_{Ai+1}\varphi_{1i+1} + \varphi'_{Ai+1}\varphi'_{1i+1}(0))]\} \\ &- D\{(\frac{\partial a_i}{\partial P})_{P_0}[\varphi_{Ai}\varphi_{1i}(0) + \varphi'_{Ai}\varphi'_{1i}(0)]\}_{i=1,N/2,N} \\ &- (Ci\omega_0/EI)(\varphi'_{AN/2+1} - \varphi'_{AN/2})(\varphi'_{1N/2+1} - \varphi'_{1N/2}); \\ C_2 &= 3D[\frac{-K_3}{2EI}(\varphi'_{AN/2+1} - \varphi'_{AN/2})(\varphi'_{1N/2+1} - \varphi'_{1N/2})^2 \\ &(\bar{\varphi}'_{1N/2+1} - \bar{\varphi}'_{1N/2})]; \\ D &= EI\, i/(2\omega_0 m); \end{aligned} \quad (41)$$

The limit cycles amplitudes obtained from equation (40) and then are plotted in Figure 12(a) for bifurcation points around the flutter point. From this Figure clearly appear that the hopf bifurcations are of supercritical (stable) type, with the steady amplitude α decreasing with K_3. Hence, the follower force has a stabilizing effect on the post-critical behavior as well as on the flutter linear boundary; and also, the curvature of the bifurcated paths changes monotonically with the bifurcation point. Similar to previous section, the nonlinearities are stronger for low values of K_3 and by increasing of K_3 nonlinearities will become weaker. In Figure 12(b), the limit cycles amplitudes α is plotted versus the stiffness K_3 for a fixed value of the parameter $\mu = 0.5$.

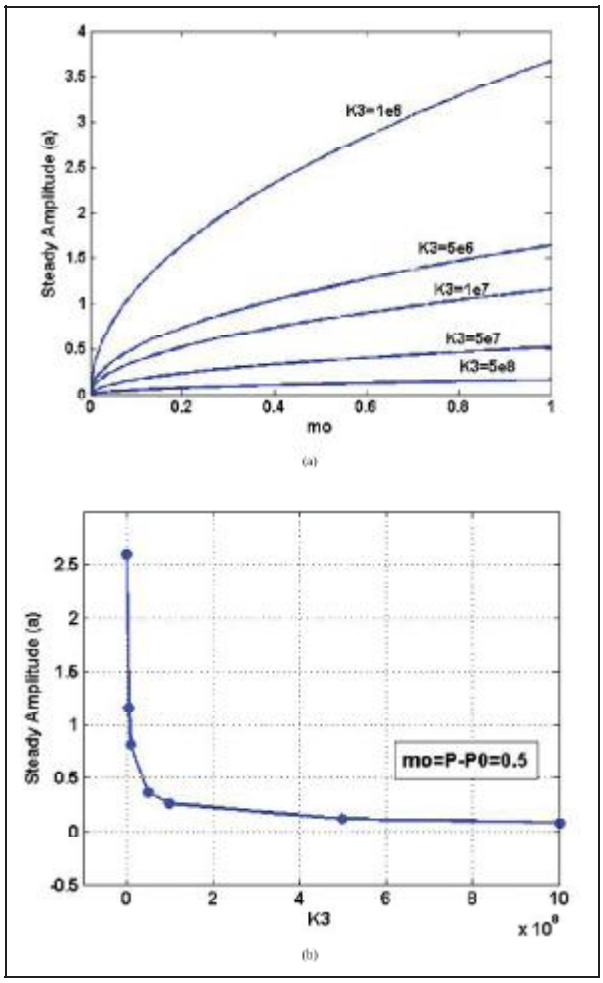

Figure 12. (a) Bifurcation diagram around different Hopf points. (b) Amplitude α versus nonlinear stiffness K3.

Conclusions

The stability of free-free jointed beams under action of nonconservative follower force has been discussed. The beam has been considered as a one-dimensional continuum model with a local rigid structure, capable of describing the mechanical behavior of the body in finite displacement regime. Nonlinear, partial differential equations of motion have been derived. The joint is combination of linear and nonlinear springs and a damper. Follower force is assumed to be linearly distributed along the length of beam, so the governing equation has variable coefficients, so, that only an approximate solution is possible.

We divided the beam to number of segment that force distributions can be approximated as constants and then we use method of multiple scale to obtain analytical solution of system.

The linear stability of the trivial equilibrium reveals the existence of buckling, flutter critical points. The spectral properties and critical modes of these two instability mechanisms have been derived and discussed. Both the nonlinearity and damping of joints have a positive effect on the stability status of the structure by decreasing the amplitude of vibration. The damping of a joint does not affect on the boundary of stability but decreases the amplitude of vibration.

The bifurcations of this problem have been analyzed. For different values of follower force the system undergoes

buckling or flutters. By using the multiple scale method, a perturbation analysis has been performed to investigate the system behavior around bifurcations in the parameter space. The relevant bifurcation equations have been numerically solved, and the whole scenario displayed in the parameter space. The analysis calls for solving two eigenvalues problems, the direct and the adjoint problems. It has been found that buckling and flutter are super-critical type close to these points.

Appendix A. Boundary and Equilibrium Conditions for Adjoint Problem

$$\int_0^L \psi(\phi'''' + P(s)\phi'')ds = \int_0^L \psi\phi''''ds + \int_0^L \psi P(s)\phi''ds = I + II \tag{A-1}$$

$$I = \int_0^L \psi\phi''''ds = \sum_{i=1}^{N}(\int_{l_{i\ 1}}^{l_i} \psi_i\phi_i^{IV}ds) = \sum_{i=1}^{N} [(\psi_i\phi_i^{III} - \psi_i'\phi_i^{II} + \psi_i^{II}\phi_i' - \psi_i^{III}\phi_i)_{l_{i\ 1}}^{l_i} + \int_{l_{i\ 1}}^{l_i} \psi_i^{IV}\phi_i ds)]$$
$$= (\sum_{i=1}^{N}(\psi_i\phi_i^{III} - \psi_i'\phi_i^{II} + \psi_i^{II}\phi_i' - \psi_i^{III}\phi_i)_{l_{i\ 1}}^{l_i}) + \int_0^L \psi''''\phi ds\,; II = \int_0^L \psi P(s)\phi''ds$$
$$= \sum_{i=1}^{N}(P_i\int_{l_{i\ 1}}^{l_i} \psi_i\phi_i^{II}ds) = \sum_{i=1}^{N} P_i[(\psi_i\phi_i' - \psi_i'\phi_i)_{l_{i\ 1}}^{l_i} + \int_{l_{i\ 1}}^{l_i} \psi_i^{II}\phi_i ds)]$$
$$= (\sum_{i=1}^{N} P_i[(\psi_i\phi_i' - \psi_i'\phi_i)_{l_{i\ 1}}^{l_i}) + \int_0^L \psi' P(s)\phi ds \tag{A-2}$$

$$I + II = \int_0^L (\psi''''\phi + \psi'' P(s))\phi\, ds + \sum_{i=1}^{N}[(\psi_i\phi_i^{III} - \psi_i'\phi_i^{II} + \psi_i^{II}\phi_i' - \psi_i^{III}\phi_i + P_i(\psi_i\phi_i' - \psi_i'\phi_i)]_{l_{i\ 1}}^{l_i}; \tag{A-3}$$
$$L^*(\psi) = \psi^{IV} + P(x)\psi^{II};$$

Boundary conditions:

$$\psi_1''(0) + a_1\psi_1(0) = 0, \qquad \psi_1'''(0) + a_1\psi_1'(0) = 0,$$
$$\psi_N''(l) + a_N\psi_N(l) = 0, \qquad \psi_N'''(l) + a_N\psi_N'(l) = 0, \tag{A-4}$$

Continuity conditions:

$$\psi_i(l) = \psi_{i+1}(0), \quad \psi_i'(l) = \psi_{i+1}'(0) \qquad i = 1 : N-1, \ \ i \neq N/2$$
$$\psi_i''(l) + a_i\psi_i(l) = \psi_{i+1}''(0) + a_{i+1}\psi_{i+1}(0),$$
$$\psi_i'''(l) + a_i\psi_i'(l) = \psi_{i+1}'''(0) + a_{i+1}\psi_{i+1}'(0), \tag{A-5}$$

Continuity conditions in joint:

$$\psi_i''(l) + a_i\psi_i(l) = \psi_{i+1}''(0) + a_{i+1}\psi_{i+1}(0), \quad i = N/2,\ \frac{K_\theta}{EI} = R,\ \frac{K_1}{EI} = Z,$$
$$\psi_i'''(l) + a_i\psi_i'(l) = \psi_{i+1}'''(0) + a_{i+1}\psi_{i+1}'(0),$$
$$\psi_{i+1}'''(0) + a_{i+1}\psi_{i+1}'(0) = Z(\psi_i(l) - \psi_{i+1}(0)),$$
$$\psi_{i+1}''(0) + a_{i+1}\psi_{i+1}(0) = R(\psi_{i+1}'(0) - \psi_i'(l)); \tag{A-6}$$

Appendix B. Boundary and Equilibrium Conditions for Bifurcation

Boundary conditions:

$$Y_{21}''(0) - a_1Y_{21}(0) = \mu(\partial a_1/\partial P)_{P_0}Y_{11}(0),$$
$$Y_{21}'''(0) - a_1Y_{21}'(0) = \mu(\partial a_1/\partial P)_{P_0}Y_{11}'(0),$$
$$Y_{2N}''(l) - a_NY_{2N}(l) = \mu(\partial a_N/\partial P)_{P_0}Y_{1N}(l),$$
$$Y_{2N}'''(l) - a_NY_{2N}'(l) = \mu(\partial a_N/\partial P)_{P_0}Y_{1N}'(l), \tag{B-1}$$

Continuity conditions:

$$Y_{2i}(l) = Y_{2i+1}(0), \qquad Y_{2i}'(l) = Y_{2i+1}'(0) \quad i = 1 : N-1, \ \ i \neq N/2$$
$$Y_{2i}''(l) - a_iY_{2i}(l) - \mu(\partial a_i/\partial P)_{P_0}Y_{1i}(l) = Y_{2i+1}''(0) - a_{i+1}Y_{2i+1}(0) - \mu(\partial a_i/\partial P)_{P_0}Y_{1i+1}(0),$$
$$Y_{2i}'''(l) - a_iY_{2i}'(l) - \mu(\partial a_i/\partial P)_{P_0}Y_{1i}'(l) = Y_{2i+1}'''(0) - a_{i+1}Y_{2i+1}'(0) - \mu(\partial a_i/\partial P)_{P_0}Y_{1i+1}'(0), \tag{B-2}$$

Continuity conditions in joint:

$$Y_{2i}''(l) - a_iY_{2i}(l) - \mu(\partial a_i/\partial P)_{P_0}Y_{1i}(l) = Y_{2i+1}''(0) - a_{i+1}Y_{2i+1}(0) - \mu(\partial a_i/\partial P)_{P_0}Y_{1i+1}(0), \ \ i = N/2$$
$$Y_{2i}'''(l) - a_iY_{2i}'(l) - \mu(\partial a_i/\partial P)_{P_0}Y_{1i}'(l) = Y_{2i+1}'''(0) - a_{i+1}Y_{2i+1}'(0) - \mu(\partial a_i/\partial P)_{P_0}Y_{1i+1}'(0),$$
$$Y_{2i}'''(l) - a_iY_{2i}'(l) = \frac{K_1}{EI}(Y_{2i}(l) - Y_{2i+1}(0)) + \mu(\partial a_i/\partial P)_{P_0}Y_{1i}'(l),$$
$$Y_{2i}''(l) - a_iY_{2i}(l) = \frac{K_\theta}{EI}(Y_{2i+1}'(0) - Y_{2i}'(l)) + \mu(\partial a_i/\partial P)_{P_0}Y_{1i}(l) + \frac{CD_0}{EI}(Y_{1i+1}'(0) - Y_{1i}'(l)) - \frac{K_3}{EI}(Y_{1i+1}'(0) - Y_{1i}'(l))^3, \tag{B-3}$$

References

Ahmadian, H. and Jalali, H., 2007, "Identification of bolted lap joints parameters in assembled structures," *Mechanical Systems and Signal Processing* 21, 1041–1050.

Barsoum, R. S., 1973, "Finite element method applied to the problem of stability of a non-conservative system," *International Journal of Numerical Methods in Engineering* 3, 63–87.

Bazant, Z. P. and Cedolin, L., 1991, *Stability of Structures*, Oxford University Press, Oxford.

Beal, T. R., 1965, "Dynamic stability of a flexible missile under constant and pulsating thrusts," *American Institute of Aeronautics and Astronautics Journal* 3, 486–495.

Bolotin, V. V., 1963, *Non-conservative Problems of Elastic Stability*, Pergamon Press, New York.

Bou-Rabee, N. M., Romero, L. A., and Salinger, A. G., "A multiparameter, numerical stability analysis of a standing cantilever conveying fluid," *SIAM Journal on Applied Dynamical Systems* 1(2), 190–214.

Herrmann, G., 1967, "Stability of equilibrium of elastic systems subjected to non-conservative forces," *Applied Mechanics Reviews* 20, 103–108.

Joshi, A., 1995, *"Free vibration characteristics of variable mass rockets having large axial thrust/acceleration". J. Sound and Vibration* 187(4), 727–726.

Langthjem, M. A. and Sugiyama, Y., 2000, "Dynamic stability of columns subjected to follower loads: a survey," *Journal of Sound and Vibration* 238 (5), 809–851.

Leipholz, H., 1980, *Stability of Elastic Systems*, Sijthoff and Noordhoff, Alphen aan den Rijn, The Netherlands.

Luongo, A., Di Egidio, A., and Paolone, A., 2002, "Multiple scale bifurcation analysis for finite-dimensional autonomous systems," *Recent Research Developments in Sound and Vibration, Transworld Research Network, Kerala, India* 1, 161–201.

Mladenov, K. A. and Sugiyama, Y., 1997, "Stability of a jointed free-free beam under end rocket thrust," *Journal of Sound and Vibration* 199, 1–15.

Nayfeh, A. H., 1973, *Perturbation Methods*, Wiley, New York.

Nayfeh, A. H. and Mook, D. T., 1979, *Nonlinear Oscillations*, Wiley, New York.

Panovko, Y. G. and Gubanova, I. I., 1965, *Stability and Oscillations of Elastic Systems*, Consultants Bureau, New York.

Paolone, A., Vasta, M., and Luongo, A., 2006a, "Flexural-torsional bifurcations of a cantilever beam under potential and circulatory forces. Part I: Nonlinear model and stability analysis," *International Journal of Nonlinear Mechanics* 41, 586–594.

Paolone, A., Vasta, M., and Luongo, A., 2006b, "Flexural-torsional bifurcations of a cantilever beam under potential and circulatory forces. Part II: Post-critical analysis," *International Journal of Nonlinear Mechanics* 41, 595–604.

Park, Y., 1985, "Dynamic stability of a free Timoshenko beam under controlled follower force," in *Proceedings of the JSME Vibration Conference*, pp. 45–53.

Park, Y. and Mote, C. D., 1985, "The maximum controlled follower force on a free-free beam carrying a concentrated mass," *Journal of Sound and Vibration* 98, 247–256.

Sundararaian, C., 1975, "The vibration and stability of elastic systems subjected to follower forces," *Shock and Vibration Digest* 7, 89–105.

Wu, J. J., 1975, "On the stability of a free-free beam under axial thrust subjected to directional control," *Journal of Sound and Vibration* 42, 45–52.

Ziegler, H., 1968, *Principles of Structural Stability*, Blaisdell, Waltham, MA.